REM sleep remains paradoxical: sub-states determined by thalamo-cortical and cortico-cortical functional connectivity

Hélène Bastuji, Maëva Daoud, Michel Magnin, Luis Garcia-Larrea

The Journal of Physiology

REM sleep remains paradoxical: sub-states determined by thalamo-cortical and cortico-cortical functional connectivity

Hélène Bastuji[1,2], Maëva Daoud[1], Michel Magnin[1] and Luis Garcia-Larrea[1]

[1]*Central Integration of Pain (NeuroPain) Lab – Lyon Neuroscience Research Center, INSERM U1028; CNRS, UMR5292, Université Claude Bernard, Bron, France*
[2]*Centre du Sommeil, Hospices Civils de Lyon, Lyon, France*

Handling Editors: Richard Carson & James Coxon

The peer review history is available in the Supporting Information section of this article (https://doi.org/10.1113/JP286074#support-information-section).

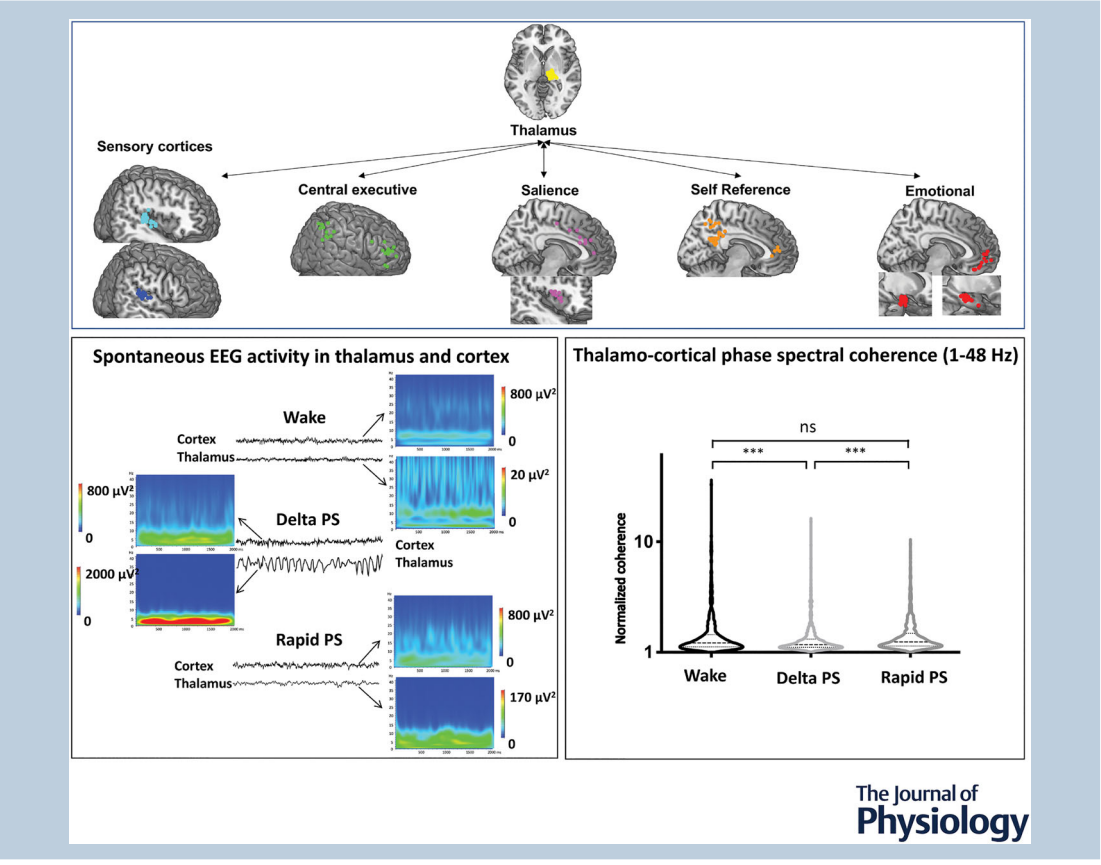

Hélène Bastuji received her MD from the University of Créteil and her PhD in Neurosciences from the University of Lyon. She is a member of the Sleep Centre at the Hospices Civils of Lyon and of the Lyon Neuroscience Research Centre, Central Integration of Pain Unit, Lyon, France. She has authored or co-authored 77 international publications and 30 didactic papers. She was a member of the Scientific Committee of the European Sleep Research Society (2001–2004) and General Secretary of the French Sleep Society (2005–2009). Her main research interests are the central integration of sensory information during human sleep, sleep and cognition, and sleep and pain.

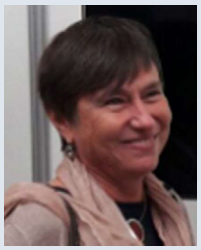

 DOI: 10.1113/JP286074

Abstract During paradoxical sleep (PS, aka REM sleep) the cerebral cortex displays rapid electroencephalographic activity similar to that of wakefulness, whereas in the posterior associative thalamus, rapid activity is interrupted by frequent periods of slow-wave (delta) oscillations at 2–3 Hz, thereby dissociating the intrinsic frequency in thalamus and cortex. Here we studied the functional consequences of such a dissociation using intrathalamic and intracortical recordings in 21 epileptic patients, applying coherence analysis to examine changes in functional connectivity between the posterior thalamus (mainly medial pulvinar) and six cortical functional networks, and also between each cortical network with respect to the others. Periods of slow-wave thalamic activity ('delta PS') were more prevalent than phases of 'rapid PS,' and the delta/rapid thalamic alternance did not overlap with the classical tonic/phasic dichotomy based on rapid eye movements. Thalamo-cortical and cortico-cortical functional connectivity significantly decreased during delta PS, relative to both rapid PS periods and to wakefulness. The fact that delta thalamic activity and low thalamo-cortical binding coincided with a suppression of cortico-cortical connectivity supports a crucial role for the posterior associative thalamus, and particularly the medial pulvinar, in ensuring trans-thalamic communication between distant cortical areas. Disruption of such a trans-thalamic communication during delta PS compromises the functional binding between cortical areas, and consequently might contribute to the alteration of perceptual experiences commonly reported during dreams.

(Received 7 December 2023; accepted after revision 16 August 2024; first published online 23 September 2024)
Corresponding author H. Bastuji: Central Integration of Pain (NeuroPain) Lab – Lyon Neuroscience Research Centre, INSERM U1028; CNRS, UMR5292; Université Claude Bernard, Bron, France. Email: bastuji@univ-lyon1.fr

Abstract figure legend Top: Localization of recording contacts used for phase spectral coherence analysis between posterior thalamus and the different areas grouped in networks: posterior insula, auditory cortex, Central Executive, Salience, Integrative (self-reference) and Emotional networks. Bottom left: iEEG signal and time frequency of cortex and thalamus during Wake, delta PS and rapid PS. Bottom right: Violin plots of antilog normalized phase coherence values during wake, delta PS and rapid PS showing that the phase coherence was significantly lower during delta PS as compared to wake and rapid PS, with no difference between rapid PS and wake.

Key points

- During paradoxical, or REM, sleep (PS), rapid thalamic activity is interrupted by frequent periods of slow delta waves at 2–3 Hz.
- During these periods of thalamic delta activity there was a drastic drop of functional connectivity between associative thalamus and cortex, and also among different cortical networks.
- The delta/rapid alternance did not overlap with the classically defined 'tonic/phasic' periods and therefore suggests a distinct dichotomy of functional states in PS.
- Recurrent decrease in thalamo-cortical and cortico-cortical functional connectivity during PS may compromise the spatio-temporal binding between cortical areas, which in turn could hinder the formation of coherent mental content during dreams.

Introduction

Paradoxical sleep (PS), aka REM sleep, first described in 1953 by Aserinsky and Kleitman in humans (Aserinsky & Kleitman, 1953) and by Jouvet in cats (Jouvet et al., 1959), is characterized by rapid low-voltage cerebral activity, muscle atonia and rapid eye movements. While the subcortical mechanisms governing the onset and arrest of PS are being gradually unravelled (Brown et al., 2012; Luppi et al., 2012; Peever & Fuller, 2017; Saper et al., 2010), the cortical activities underlying one of its most obvious features, namely the mental activity reflected by dreams, remain elusive (Casaglia & Luppi, 2022; Nir & Tononi, 2010; Wang et al., 2022). PS is the period of sleep during which the most vivid dreams occur (Hobson, 2009; Simor et al., 2023), the contents of which depend on underlying cortical processes, as witnessed by 'lucid dreamers' (Dresler et al., 2011; Oudiette et al., 2018) and patients with 'REM sleep behaviour disorder' who act out their dreams (Arnulf, 2012; Mahowald & Schenck, 2004).

Studies focusing on dream reports have shown that their cognitive content is patterned by inconstancy in time, place and person, with associations of disparate and incongruous elements akin to confabulation (Hobson, 1997, 2004). These elements show striking similarities with traits observed in the context of some neuropsychological conditions (Schwartz & Maquet, 2002); in particular, disconnection syndromes where the contextual interpretation of external events is obstructed by a failure of communication between brain areas (Dalla Barba et al., 2018; Schnider et al., 1996). A similar deficit in communication between brain areas has also been suggested during PS, via a decreased correlation of both haemodynamic and electrophysiological signals between sensory regions and high-order areas (Chow et al., 2013; Corsi-Cabrera, 2003; Nir & Tononi, 2010).

In addition to the well-known phasic and tonic periods of PS, defined by the presence or not of rapid eye movements (Simor et al., 2020), another functional dichotomy has been reported based on recordings in the human posterior thalamus (Velasco et al., 1979), consisting of alternating periods of rapid thalamic activity ('rapid PS') interrupted by recurrent episodes of low-frequency delta oscillations ('delta PS') at 2–3 Hz. During the rapid PS periods, thalamic activity is similar to that recorded in cortical areas, whereas during delta PS periods the slow thalamic oscillations contrast with the persistent rapid activity within the cerebral cortex (Magnin et al., 2004). These slow periods involve a major associative thalamic nucleus, the medial pulvinar (PuM), which is considered to be a critical node for the trans-thalamic routing of information between distant cortical areas (Baleydier & Mauguiere, 1985; Cappe et al., 2009; Froesel et al., 2021; Morel et al., 1997; Shipp, 2003). This suggests that the irruption of such slow periods may interfere with the PuM capability to ensure a coherent thalamo-cortical and cortico-cortical functional connectivity.

In this study we used intrathalamic and intracortical recordings in humans during all-night sleep, to explore the patterns of thalamo-cortical and cortico-cortical connectivity during alternating periods of delta and rapid PS thalamic activities. Our working hypothesis was that dissociation between thalamic activities and their related cortical areas should compromise the thalamo-cortical functional coupling, and possibly also induce a functional disconnection between cortical areas via the disruption of their trans-thalamic functional connectivity.

Methods

Patients

Ethical approval. In agreement with French regulations for invasive investigations with direct individual benefit, patients included in this study were fully informed about electrode implantation, stereotactic EEG (iEEG) and the cortical stimulation procedures used to localize the epileptogenic cortical areas and gave their written consent. The procedure was approved by the national Ethics Committee (Comité de Protection des Personnes Sud-Est IV n° 2006-A00572-49 and III no. 2014-A01280−47) and was in accordance with the 1964 *Declaration of Helsinki* and its later amendment, except for registration in a database.

Twenty-one patients with refractory partial epilepsy were included in this study (14 men, 7 women; mean age 33 years, range 19–51 years). To delineate the extent of the cortical epileptogenic area and to plan a tailored surgical treatment, depth EEG recording electrodes (diameter 0.8 mm; 5–15 recording contacts 2 mm long; inter-contact interval 1.5 mm) were implanted orthogonally according to the Talairach space.

Night sleep recordings from each patient were collected after a minimal delay of 5 days after electrode implantation; at that time, any 'first-night' effect had faded away, and antiepileptic drugs had been tapered down with daily smaller doses or stopped (see Table 1).

Electrode implantation. Intracerebral electrodes were implanted using the Talairach stereotactic frame. A cerebral angiography was performed in stereotactic conditions using an X-ray source located 4.85 m from the patient's head. This eliminates the linear enlargement due to X-ray divergence and allows a 1:1 scale so that the films could be used for measurements without any correction. In a second step, the relevant targets were identified on the patient's magnetic resonance image (MRI), previously enlarged to a scale of one to one. As the magnetic resonance and angiographic images were at the same scale, they could easily be superimposed, to avoid damage to blood vessels and minimize the risk of haemorrhage during electrode implantation.

Anatomical localization of electrode contacts. Localization of the recording contacts was determined using two different procedures. In seven patients implanted before 2010, MRI could not be performed with electrodes *in situ* because of the physical characteristics of stainless-steel contacts. In these cases, the scale 1:1 post-implantation skull radiographs performed within the Talairach stereotactic frame were superimposed on the pre-implantation scale 1:1 MRI slice corresponding to each electrode track, thus permitting each contact to be plotted on the appropriate MRI slice of each patient and to determine its coordinates (MRIcro software; Rorden & Brett, 2000). In the other 14 patients, the implanted electrodes were MRI-compatible, and contacts could be directly visualized on the post-operative 3D MRIs. In

Table 1. Individual clinical, MRI and iEEG data

Patient	Sex/age	Treatment	MRI	Seizure onset	Number of electro-des/left, right
P1	M/20	Valproate 500 Carbamazepine 600 Levetiracetam 1000	L temporal atrophy	L temporal	13/L
P2	M/33	Carbamazepine 600 Lamotrigine 200 Lacosamide 100	Normal	L temporal	12/L+2/R
P3	M/36	Levetiracetam 750	R hippocampal atrophy	R temporal	12/R
P4	M/40	None	L temporal atrophy	L mesial temporal	10/L
P5	F/49	Levetiracetam 1000 Lacosamide 100	R temporal dysplasia	R mesial temporal	13/R
P6	F/30	Eslicarbazepine 400 Lacosamide 100	Normal	L operculo insular	12/L
P7	M/19	None	Normal	R mesial temporal	11/R
P8	F/37	Carbamazepine 600 Pregabalin 75	Normal	L mesial temporal	13/L
P9	M/35	None	Normal	R temporo-parieto-occipital junction	10/R+5/L
P10	M/37	Carbamazepine 400 Topiramate 200 Clobazam 5	Normal	L perisylvian	13/L
P11	M/19	Carbamazepine 800 Valproate 500 Clobazam 10	R fronto-orbital dysplasia	R fronto-orbital	11/R
P12	M/36	Levetiracetam 1000 Lacosamide 100	L amygdala atrophy	L basal temporal	12/L+2/R
P13	F/23	Levetiracetam 1000 Lamotrigine 300	L hippocampal atrophy	L mesial temporal	11/L
P14	M/39	Lamotrigine 200 Topiramate 200 Levetiracetam 1000 Lacosamide 100	L hippocampal atrophy	L mesial temporal	11/L
P15	M/26	Carbamazepine 200 Lamotrigine 200 Pregabalin 75	L hippocampal atrophy	L mesial temporal	12/L
P16	M/32	Levetiracetam 1000 Oxcarbazepine 150	L hippocampal atrophy	L basal temporal	13/L+2/R
P17	F/51	Oxcarbazepine 200 Clobazam 10	Normal	R temporal	12/R
P18	F/43	Carbamazepine 400 Topiramate 200	R hippocampal atrophy	R mesial temporal	9/R+2L
P19	F/31	Valproate 500 Topiramate 10	L temporal dysplasia	L temporal	15/L
P20	M/41	Lamotrigine 350 Levetiracetam 1000 Carbamazepine 200	R hippocampal atrophy	R hippocampus	15/R
P21	M/21	Topiramate 200 Oxcarbazepine 900 Lamotrigine 400	R temporal dysplasia	R temporal	11/R+3/L

both cases, anatomical scans were acquired on a 3-Tesla Siemens Avanto Scanner using a 3D MPRAGE sequence with following parameters: TI/TR/TE 1100/2040/2.95 ms, voxel size: $1 \times 1 \times 1$ mm^3, FOV $= 256 \times 256$ mm^2.

Intrathalamic electrode contacts. In this work we followed the thalamic nuclei nomenclature of Hirai and Jones (1989), Morel et al. (1997) and Krauth et al. (2010). The localization of the contacts within the thalamic nuclei was performed with the appropriate MRI slice of each patient and the Morel stereotactic atlas of the human thalamus (Morel et al., 1997). In the 14 patients with MRI-compatible electrodes, contacts could be localized according to their positions with respect to the anatomy of each patient, and then projected onto the thalamic atlas. In the seven patients without MRI-compatible electrodes, the coordinates of contacts were determined on their own MRI in accordance with the procedure described above. In these cases, even after correction for contact locations and evaluation on an individual patient's MRI, the contact localization is prone to inaccuracies linked to MRI slice thickness ($\pm$0.5 mm), superimposition of the MRI slice on the X-ray ($\pm$1 mm) and coordinate measurements ($\pm$0.5 mm), which lead to an average error (square root of the sum of the squares of the different errors) of $\pm$1.32 mm in anteroposterior and dorsoventral dimensions, and $\pm$1.11 mm in the mediolateral dimension (Bastuji et al., 2016; Rosenberg et al., 2006). We therefore checked in each patient that, even accounting for these possible errors, none of the thalamic contacts could be located outside the thalamic nuclei considered.

Intracortical electrode contacts. Intracortical electrode contacts were mapped into the standard stereotaxic space (Montreal Neurological Institute, MNI) by processing MRI data with Statistical Parametric Mapping (SPM12 — Wellcome Department of Cognitive Neurology, UK; http://www.fil.ion.ucl.ac.uk/spm/). Anatomical T1-3D images pre- and post-implantation were co-registered and normalized to the MNI template brain image using a mutual information approach and the segmentation module of SPM12, which segments, corrects bias and spatially normalizes images with respect to the MNI model. Then, the cortical localization of electrodes was performed using regional atlas (WFU Pickatlas v3) in MRIcro. In the 14 patients with MRI-compatible electrodes, the cortical contacts could be directly visualized on the post-operative normalized 3D MRIs. In the seven patients without MRI-compatible electrodes, the coordinates of contacts were determined on their own MRI following to the procedure described above, thus permitting each contact to be plotted on the appropriate MRI slice of each patient (MRIcron software; Rorden & Brett, 2000), to determine its MNI coordinates and to check its localization on the Brodmann atlas. A specific atlas of the human insula (Faillenot et al., 2017) was used to localize and verify the contacts in this structure.

Data acquisition and recording procedure. Recordings were performed in common referential mode using a reference electrode contact located in the skull. Night EEG was recorded continuously at a sampling frequency of 256 Hz or 512 Hz from 96 to 128 channels, amplified and band-pass filtered (0.33–128 Hz; $-$3 dB, 12 dB/octave) to be stored on a hard disk for offline analysis (Micromed SAS, Macon France).

Detection and selection of wake and paradoxical sleep. The criteria of the American Academy of Sleep Medicine adapted to intracerebral recordings (Magnin et al., 2004, 2010) were used for the iEEG data. Then, two periods of 5 min were selected for each patient, one during wake and the other during PS. The periods for wake were selected in the pre-sleep EEG and those for PS in the second half of the night during which PS phases are more stable. This allowed us to obtain the 150 PS segments of 2 s each needed to perform the connectivity analysis. Analyses were performed offline using BrainVision System (Brain Products, Munich, Germany). Before EEG segmentation, PS periods with delta activity (delta PS) and those with high-frequency activity (rapid PS) in the thalamic contacts were identified (Fig. 1). Then, the 50 Hz notch-filtered EEG signal (wake, delta PS and rapid PS) was divided into 2 s segments. Segments containing artefacts as well as recordings from any electrode contact situated in lesioned areas or detecting epileptic anomalies were discarded. A low-pass filter at 0.5 Hz with a slope of 24 dB/octave was then applied before performing the spectral analysis. The coordinates of the cerebral contacts kept for analysis using both monopolar (referential) and bipolar montages are indicated in Table 2.

Electrophysiological data and statistical analyses. A Fourier transform was performed on EEG signals in referential mode, to convert data from the time domain to the frequency domain. Then, the power of EEG signals was assessed according to each frequency band (delta, theta, alpha, beta and low gamma). For each patient, the spectral contents of all segments recorded in each vigilance stage (wake, delta PS or rapid PS) were averaged. When located in the same structure, these averaged spectral contents were combined into one grand mean.

Functional connectivity was studied using phase-coherence analysis between the posterior thalamus ('seed region') and the cortical areas recorded (Fig. 2). Coherence was performed after a fast Fourier transform of the signal for each spectral band power (δ: 1–3 Hz, θ: 4–7 Hz, α: 8–12 Hz, β: 13–29 Hz, low γ: 30–48 Hz)

Table 2. Montreal Neurological Institute coordinates (x,y,z) of cerebral contacts

Contacts	P insula (*n* = 20)	Audit C (*n* = 18)	DLPFC (*n* = 13)	PPC (*n* = 11)	ACC (*n* = 4)	MCC (*n* = 5)	A insula (*n* = 8)	PCC (*n* = 14)	pACC (*n* = 5)	Precun (*n* = 7)	Hippo (*n* = 12)	Amyg (*n* = 15)	OFC (*n* = 11)	Thal (*n* = 21)
Patients														
P1	38,−16,17	33,−29,8	38,41,6	39,−55,50	4,41,6		35,0,11	3,−39,30		3,−57,49		18,−3,−20	9,53,−9	12,−29,8
P2	39; −5; −3		41,37,−15								29,−17,−18	21,−6,−16	8,40,−16	15,−28,−4
P3	39,−19,2	53,−19,2	37,54,15						7,33,0		21,−11,−21	26,−3,−17	3,35,−19	11,−19,3
P4		45,−25,7										21,−1,−21		20,−25,7
P5	38,−8,0		48,42,−13			6,21,19						23,−7,−27	7,45,−14	16,−21,10
P6	35,−16,17	57,−25, 7		41,−47,37		9,7,37	34,0,13	10,−48,26						11,−27,5
P7	36,−8,17	60,−9,2	38,33,−18				36,11,2		7,44,10		27,−16,−20	25,−2,−22	6,35,−20	10,−21,7
P8	35,−26,27	45,−23,5	28,46,23	33,−50,46		4,22,28	33,6,12	4,−50,20		5,−51,44	31,−20,−16		5,46,−17	8,−23,5
P9	40,−21,7	44,−23,6	30,39,24	39,−36,37	7,38,24			10,−55,24			29,−17,−16			12,−21,7
P10	37,−12,2	47,−27,6	42,48,9				35,8,5		8,46,7		27,−16,−14	23,−2,−21	7,48,−11	11,−27,5
P11	37,−20,5	52,−25,8			4,29,22			5,−48,18		5,−48,56	25,−16,−20	21,−3,−18		23,−28,8
P12	39,−5,−4	40,−24,6	31,53,1					9,−43,25			24,−15,−16	21,−4,−21	5,52,1	15,−24,6
P13	37,−24,2	46,−31,8		34,−50,38				3,−48,23		8,−53,41		20,−6,−23		14,−29,8
P14	36,−25,1	41,−26,1		40,−61,45				9,−52,26		14,−63,45		21,−9,−26		14,−26,1
P15	33,−24,5	43,−24,5	30,44,11				32,2,8		5,44,14					12,−24,4
P16	36,−12,−1	49,−23,6	29,56,1					6,−42,31			29,−18,−16	17,0,−11	4,54,1	11,−26,4
P17	37,−1,−4	57,−27,9		54,−45,29			38,16,1	10,−45,25			22,−15,−25	15,−6,−20	5,37,−21	11,−25,8
P18	35,−22,7	60,−22,7		47,−40,31				5,−42,31			23,−17,−14	15,−3,−28		13,−24,5
P19	42,−29,9	49,−29,9	36,51,9	46,−45,50	6,30,20	7,−10,48		7,−43,34		6,−43,46				12,−29,5
P20	41,−8,−12		45,38,4	60,−44,31				9,−40,31	8,40,8			20,−6,−17	6,41,−14	8,−24,4
P21	38,−23,9	45,−23,9		43,−58,49		7,17,37	37,−8,19	8,−57,25		8,−57,51	29,−18,−16			15,−21,9
Mean	37,−16,5	48,−24,6	36,45,4	43,−48,40	5,35,18	7,11,34	35,4,9	7,−47,26	7,41,8	7,−53,47	26,−16,−18	20,−4,−21	6,44,−13	13,−25,5
SD	2,8,9	7,5,2	3,7,13	8,8,8	2,6,8	2,13,11	2,7,6	3,6,5	1,5,5	4,7,5	3,2,3	3,2,4	2,7,8	4,3,3

P insula: posterior insula; audit C: auditory cortex; DLPFC: dorsolateral prefrontal cortex; PPC: posterior parietal cortex; ACC: anterior cingulate cortex; MCC: median cingulate cortex; A insula: anterior insula; PCC: posterior cingulate cortex; precun: precuneus; hippo: hippocampus; amyg: amygdala; OFC: orbitofrontal cortex; thal: thalamus.

with a resolution of 1 Hz. The phase coherence between each pair of electrode contacts was calculated using the quotient between cross-spectral and auto-spectral density functions for each frequency and each channel. After Fisher's Z-transformation of phase-coherence data to approach normalized Z-values for each patient, the values remained non-fully normally distributed, with significant skewness but homogeneous variances. Then, we compared the Z-transformed coherence values among the three states of vigilance (wake, delta PS, rapid PS) in

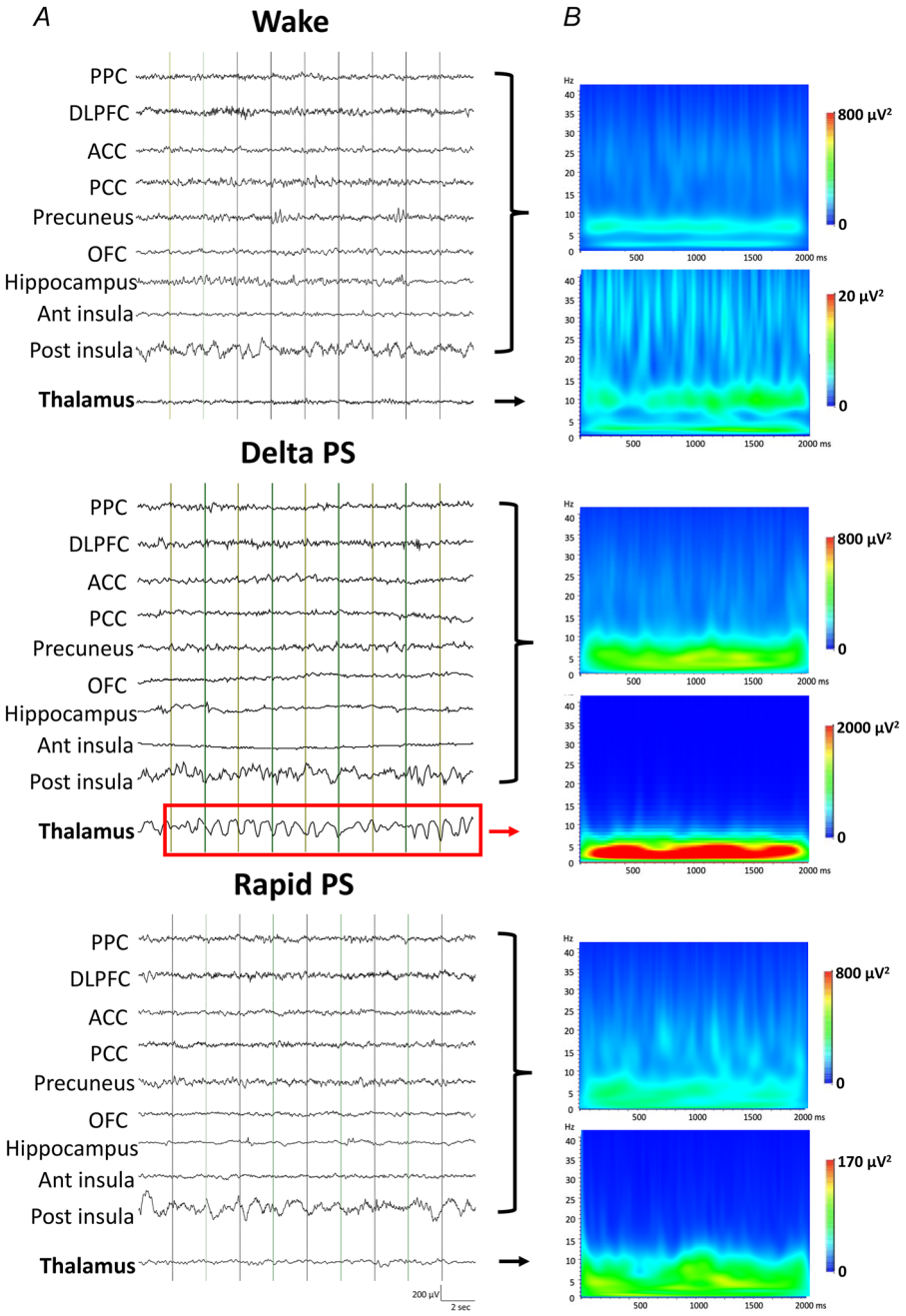

Figure 1. Cortical and thalamic EEG activities during wake, delta PS and rapide PS
A, examples of iEEG signals in one patient obtained during wake (top), delta paradoxical sleep (PS) (middle) and rapid PS (bottom) in various cerebral areas and thalamus. PPC: posterior parietal cortex; DLPFC: dorsolateral prefrontal cortex; ACC: anterior cingular cortex; PCC: posterior cingular cortex; OFC: orbitofrontal cortex. Note the slow activity of high amplitude in the delta range frequency present in the thalamic contact, characteristics of delta PS. *B*, grand means of time frequency signals of thalamus (bottom) and other cerebral areas (top) during wake, delta PS and rapid PS. Note that, while for the cortex the colour scales are the same, in the case of thalamus the scale is much higher during delta PS (2000 μV^2) than during wake (20 μV^2) and rapid PS (170 μV^2).

all frequency bands and cortical areas separately for each patient.

To improve the power of the analysis and according to the literature, the cortical areas were clustered into six parcels (two sensory areas and four functional networks, Fig. 2*A*). The two sensory areas were the auditory cortex, including primary and secondary areas, and the posterior insula, receiving mainly somatosensory inputs (Friedman et al., 1986). The functional networks considered were based on previous literature (see Doucet et al., 2019; Menon, 2011; Uddin et al., 2019) and comprised (1) a 'central executive' network including the dorsolateral prefrontal cortex and the posterior parietal cortex, which are responsible for multiple control functions in response to internal or external stimuli (sustained attention, working memory manipulation, decision making, goal-oriented planning) (Seeley, 2010); (2) a 'salience network' (anterior insula, median cingulate cortex, anterior cingulate cortex), implicated in the detection of and oriented toward salient stimuli, conflict monitoring and response selection (Frot et al., 2022; Heine et al., 2012); (3) a 'self-reference', late-integrative

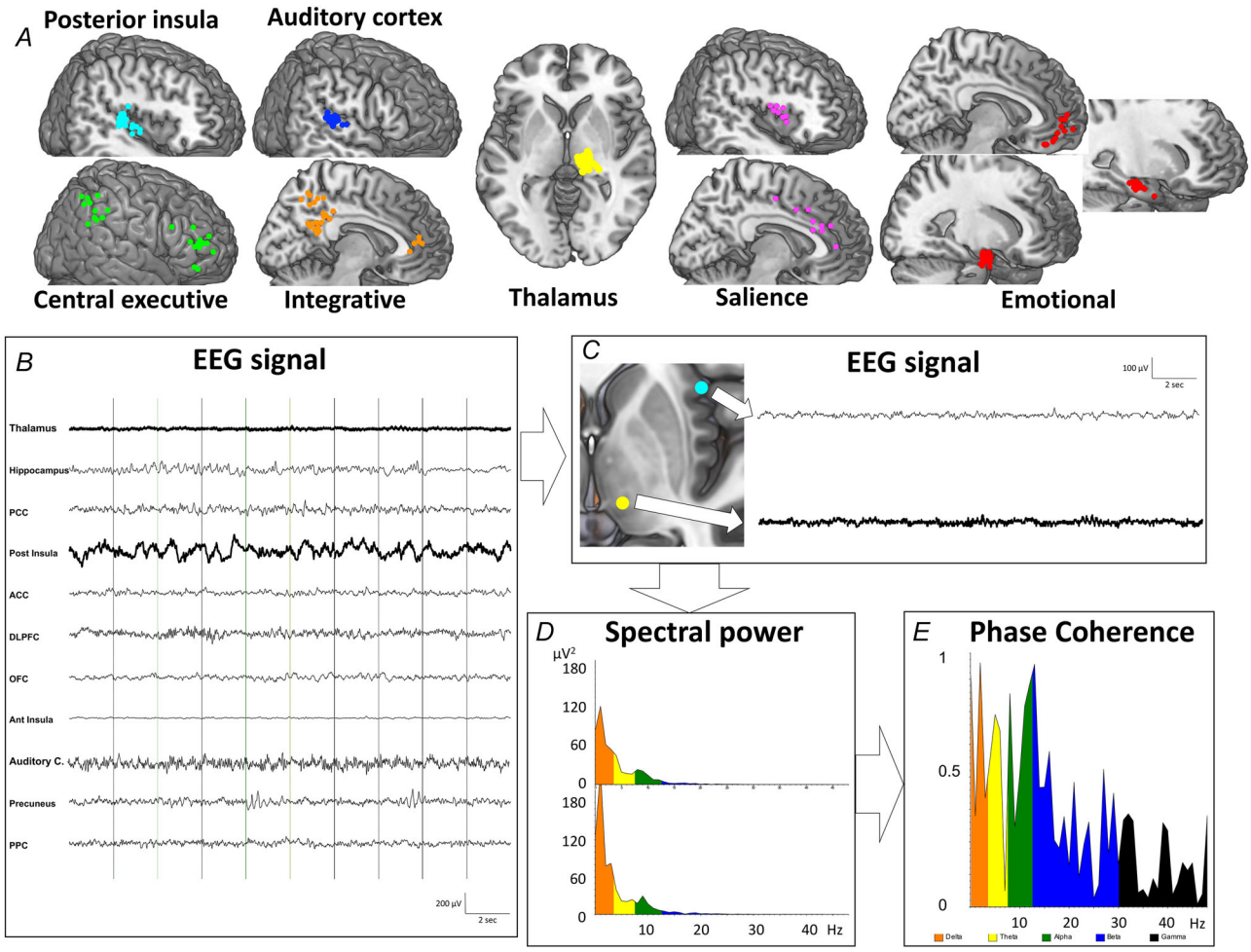

Figure 2. Localization of cerebral contacts used for spectral phase coherence
A, localization of recording contacts used for analysis in each area represented on Montreal Neurological Institute brain templates: *Left*, *top*, sagittal slice with contacts in posterior insula (cyan) (n = 20), sagittal slice with contacts in auditory cortex (blue) (n = 18); *left, bottom*, brain convexity with contacts in the central executive network including the dorsolateral prefrontal cortex and posterior parietal cortex (green) (n = 24), mid-sagittal slice with contacts in integrative (self-reference) network including the pregenual cingulate cortex, posterior cingular cortex and precuneus (orange) (n = 26); *Middle*, axial slice with contacts in the posterior thalamus (yellow) (n = 21); *Right*, *left*, sagittal and mid-sagittal slices with contacts in the salience network including anterior insula, anterior cingular cortex and median cingulate cortex (magenta) (n = 17); *right, right*, sagittal slices with contacts in emotional network including amygdala, hippocampus and orbitofrontal cortex (red) (n = 38). *B*, example of iEEG traces in 11 areas. *C*, two iEEG signals, one in the thalamus and the other in the posterior insula. On the MRI slice yellow and cyan circles represent the localization of these two contacts. *D*, spectral powers of both iEEG signals. *E*, phase coherence between the thalamus signal and the one simultaneously recorded in the posterior insula.

network focused on autobiographical memory and integration of cognitive processes, encompassing the precuneus, the posterior cingulate cortex and the pregenual cingulate cortex (Whitfield-Gabrieli et al., 2011), and (4) an 'emotional network' composed of the amygdala, the orbitofrontal cortex and the ventral hippocampus (Fanselow & Dong, 2010; John et al., 2013).

Phase-coherence values between the thalamus and the different sensory areas/networks were submitted to a three-way mixed ANOVA with 'frequency band' and 'state of vigilance' as within factors and 'network' as between factors. Similar ANOVAs were performed for phase-coherence values between each sensory area/network ('seed') with respect to all the others. Bonferroni correction was applied to the main ANOVA effects, and *post hoc t* tests (Holm–Sidak's test also corrected for multiple comparisons) were applied in the event of significant effects following ANOVA. Given the multiple cortico-cortical ANOVA comparisons, significant main effect thresholds were Bonferroni-corrected (significance threshold set at $P < 0.0083$ to obtain an overall $P < 0.05$ value). Effect sizes were estimated using η^2_p for ANOVA and Cohen's d for *t* tests.

To further assess the specificity of the results, we compared them to a 'null model' that preserved spectral content but scrambled the coherence of the data, using a control ANOVA with identical design as above, but conducted on randomly scattered values of phase coherence between the thalamus and the different sensory networks.

Correlation matrices of coherence values between all individual areas included in the networks were also derived from the data, and the percentage of significant coherence values between areas (i.e. values higher than 0.2 (Achermann & Borbély, 1998; Bastuji et al., 2016)) compared across different states using Fisher's exact tests.

In a subgroup of eight patients in whom electro-oculograms were good enough quality, the classical phasic and tonic periods were also determined using the usual criteria and the segments classified as delta-tonic, delta-phasic, rapid-tonic and rapid-phasic. Too few segments could be obtained corresponding to the rapid-phasic combination (three to eight segments per patient) precluding a reliable estimation of phase-coherence values. Thus, only the spectral phase-coherence data between delta and rapid periods occurring during tonic PS could be reliably compared.

Results

Functional connectivity was studied using spectral phase-coherence analysis between the posterior thalamus as 'seed region' (medial pulvinar in 86% of the cases, central lateral in 14%) and the cortical networks, and between each cortical network with the others during waking, delta PS and rapid PS (Figs 1 and 2). The periods of thalamic delta activity represented 75.5 (8.3)% of the total PS time. A total of 2253 iEEG segments were analysed: 40 (13) segments of wake, 38 (16) segments of delta PS and 29 (10) segments of rapid PS per patient.

Table 3. *Post hoc* analyses of the network factor on thalamo-cortical phase coherence. *t*, *P* and *d* values if significant

Networks	*t*	*P*	*d*
PI *vs.* AU	6.83	**<0.0001**	**0.69**
PI *vs.* CE	4.03	**0.0005**	**0.32**
PI *vs.* SA	5.34	**<0.0001**	**0.30**
PI *vs.* IN	3.46	**0.0034**	**0.28**
PI *vs.* EM	5.49	**<0.0001**	**0.43**
AU *vs.* CE	3.21	**0.0068**	**0.35**
AU *vs.* SA	11.77	**<0.0001**	**0.76**
AU *vs.* IN	3.89	**0.0007**	**0.45**
AU *vs.* EM	2.46	0.055 ns	/
CE *vs.* SA	9.40	**<0.0001**	**0.53**
CE *vs.* IN	0.68	0.50 ns	/
CE *vs.* EM	1.14	0.45 ns	/
SA *vs.* IN	8.94	**<0.0001**	**0.51**
SA *vs.* EM	11.23	**<0.0001**	**0.60**
IN *vs.* EM	1.92	0.16	/

PI: posterior insula; AU: auditory cortex; CE: central executive; SA: salience; IN: integrative ('self-reference'); EM: emotional.

Thalamo-cortical spectral phase coherence during wake, delta PS and rapid PS

Results are summarized in Fig. 3. ANOVA on phase coherences between thalamus and the different functional networks revealed significant effects of the state of vigilance ($F(2,137) = 23.96$; $P < 0.0001$; $\eta^2_p = 0.15$), network ($F(5,137) = 5.97$; $P < 0.0001$; $\eta^2_p = 0.18$) and frequency band ($F(4,137) = 26.14$; $P < 0.0001$; $\eta^2_p = 0.16$). There were significant interactions between state*band ($F(8,274) = 6.74$; $P < 0.0001$; $\eta^2_p = 0.05$), state*network ($F(10,274) = 1.97$; $P = 0.036$; $\eta^2_p = 0.01$) and network*band ($F(20,548) = 2.25$; $P = 0.0015$; $\eta^2_p = 0.03$).

Post hoc analyses showed that thalamo-cortical phase coherence was significantly decreased during delta PS as compared with both wake ($t(714) = 6.30$; $d = 0.24$; $P < 0.0001$) and rapid PS ($t(714) = 9.09$; $d = 0.28$; $P < 0.0001$), with no difference between the two latter ($t(714) = 0.22$; $P = 0.83$ ns). The thalamus had highest coherence levels with the salience network, and lowest with the auditory area (Table 3). Thalamo-cortical phase coherence decreased with increasing frequency range: it

was significantly higher for the delta band as compared with the other bands; for theta and alpha as compared with beta and gamma; and for beta as compared with gamma (Table 4).

Thus, in all the regions and networks studied, thalamo-cortical spectral phase-coherence levels were significantly attenuated during delta PS as compared with rapid PS (Table 5), and depressed relative to wake in all areas/networks except in auditory regions and the emotional network. Thalamo-cortical phase coherence was similar in rapid PS and wake (Fig. 3 and Table 6). The interaction between networks and frequency bands is detailed in Table 7.

The 'null model' control ANOVA based on random phase-coherence values between the thalamus and the different sensory areas/networks showed no significant

Table 4. *Post hoc* analyses of the frequency band factor on thalamo-cortical phase coherence. *t*, *P* and *d* values if significant

Band	*t*	*P*	*d*
Delta *vs.* theta	6.32	**<0.0001**	**0.28**
Delta *vs.* alpha	5.24	**<0.0001**	**0.27**
Delta *vs.* beta	7.30	**<0.0001**	**0.43**
Delta *vs.* gamma	8.58	**<0.0001**	**0.54**
Theta *vs.* alpha	0.18	0.86 ns	
Theta *vs.* beta	3.63	**0.0009**	**0.17**
Theta *vs.* gamma	5.37	**<0.0001**	**0.29**
Alpha *vs.* beta	5.22	**<0.0001**	**0.18**
Alpha *vs.* gamma	6.06	**<0.0001**	**0.29**
Beta *vs.* gamma	3.29	**0.0022**	**0.14**

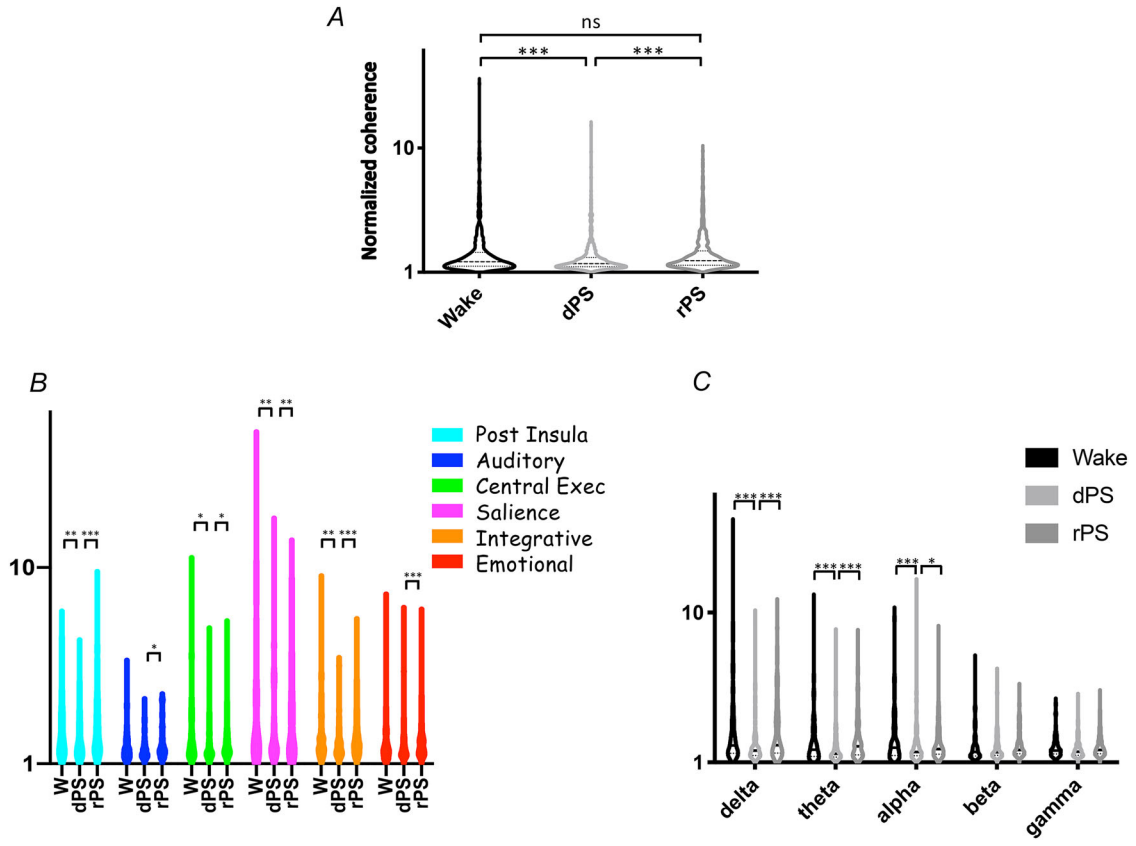

Figure 3. Phase coherence between thalamus and the other sensory areas/networks
A, violin plots of antilog normalized phase-coherence values (n = 715) during wake, delta paradoxical sleep (PS) and rapid PS showing that the phase coherence was significantly lower during delta PS as compared with wake and rapid PS, with no difference between rapid PS and wake. *B*, violin plots of antilog normalized phase-coherence values of the interaction between the state of vigilance and the sensory areas/networks showing that the phase coherence of the thalamus was significantly decreased during delta PS as compared with rapid PS with all networks, and as compared with waking with posterior insula (n = 100), central executive (n = 120), salience (n = 85) and integrative (self-reference) (n = 130) networks, but not with auditory (n = 90) and emotional (n = 190) ones; there were no significant differences between rapid PS and waking with all sensory areas/networks. *C*, violin plots of antilog normalized phase-coherence values (n = 143) of the interaction between the state of vigilance and the frequency bands showing that the phase coherence was significantly lower during delta PS as compared with wake and rapid PS for delta, theta and alpha, but not for beta and gamma.

Table 5. *Post hoc* analyses of the interaction between state and frequency band on thalamo-cortical phase coherence. *t, P* and *d* values if significant

Band	delta	Theta	alpha	beta	gamma
dPS *vs*. wake	8.19; **<0.0001; 0.39**	3.64; **0.0006; 0.25**	4.22; **<0.0001; 0.27**	1.16; 0.43	0.81; 0.66
dPS *vs*. rPS	7.38; **<0.0001; 0.40**	5.18; **<0.0001; 0.38**	2.66; **0.016; 0.19**	1.80; 0.20	1.57; 0.31
rPS *vs*. wake	0.81; 0.41	1.55; 0.12	1.56; 0.12	0.64; 0.52	0.75; 0.66

dPS: delta paradoxical sleep; rPS: rapid paradoxical sleep.

Table 6. *Post hoc* analyses of the interaction between state and network on thalamo-cortical phase coherence. *t, P* and *d* values if significant

Network	PI	AU	CE	SA	IN	EM
dPS *vs*. wake	3.58; **0.0011; 0.40**	2; 0.096	2.60; **0.021; 0.25**	3.33; **0.0026; 0.37**	2.95; **0.0076; 0.33**	1.16; 0.25
dPS *vs*. rPS	4.60; **<0.0001 0.44**	2.49; **0.043; 0.28**	2.97; **0.01; 0.21**	3.66; **0.0013; 0.30**	4.95; **<0.0001; 0.42**	3.91; **0.0004; 0.21**
rPS *vs*. wake	0.65; 0.52	0.13; 0.90	0.64; 0.52	1.26; 0.21	0.42; 0.67	1.82; 0.14

PI: posterior insula; AU: auditory cortex; CE: central executive; SA: salience; IN: integrative ('self-reference'); EM: emotional; dPS: delta paradoxical sleep; rPS: rapid paradoxical sleep.

Table 7. *Post hoc* analyses of the interaction between network and frequency band on thalamo-cortical phase coherence. *t, P* and *d* values if significant

Network	PI	AU	CE	SA	IN	EM
Delta *vs*. theta	1.11; 0.74	1.59; 0.64	2.96; **0.012; 0.37**	2.01; 0.18	3.88; **0.0016; 0.50**	4.23; **0.0005; 0.35**
Delta *vs*. alpha	1.04; 0.74	1.42; 0.66	3.32; **0.0057; 0.47**	1.35; 0.33	4.05; **0.001; 0.57**	2.07; 0.25
Delta *vs*. beta	1.51; 0.59	2.23; 0.26	5.02; **<0.0001; 0.76**	3.25; **0.014; 0.54**	4.36; **0.004; 0.67**	1.83; 0.30
Delta *vs*. gamma	2.58; 0.12	1.16; 0.69	4.98; **<0.0001; 0.76**	3.68; **0.0046; 0.67**	5.02; **<0.0001; 0.80**	3.52; **0.0056; 0.43**
Theta *vs*. alpha	0.16; 0.87	0.15; 1.00	1.14; 0.45	0.47; 0.64	0.72; 0.47	1.70; 0.30
Theta *vs*. beta	0.92; 0.74	1.45; 0.66	4.841; **0.0003; 0.60**	2.83; **0.033; 0.33**	1.53; 0.34	1.91; 0.30
Theta *vs*. gamma	2.08; 0.29	0.09; 1.00	4.99; <0.0001; 0.59	3.17; **0.0155; 0.048**	2.74; **0.045; 0.40**	0.39; 0.91
Alpha *vs*. beta	1.20; 0.74	1.90; 0.44	4.34; **0.0003; 0.53**	4.45; **0.0005; 0.37**	1.31; 0.35	0.29; 0.91
Alpha *vs*. gamma	2.43; 0.15	0.02; 1.00	4.18; **0.0004; 0.51**	3.89; **0.0027; 0.51**	2.35; 0.10	1.92; 0.30
Beta *vs*. gamma	1.89; 0.37	1.49; 0.66	0.15; 0.88	1.79; 0.22	2.01; 0.18	2.58; 0.09

PI: posterior insula; AU: auditory cortex; CE: central executive; SA: salience; IN: integrative ('self-reference'); EM: emotional.

differences for any of the factors: state of vigilance ($F(2,137) = 0.29$; $P = 0.74$), network ($F(5,137) = 0.59$; $P = 0.71$) and frequency band ($F(4,137) = 0.19$; $P = 0.95$).

Cortico-cortical spectral phase coherence during wake, delta PS and rapid PS

ANOVA showed a Bonferroni-corrected significant effect of the state of vigilance on the spectral phase coherences between each functional network ('seed region') and the other networks. Seeds were the posterior insula ($F(2,116) = 16.60$; $P < 0.0001$; $\eta^2_P = 0.13$); the auditory cortex ($F(2,103) = 16.66$; $P < 0.0001$; $\eta^2_P = 0.14$), the 'central executive' network ($F(2,135) = 12.20$; $P < 0.0001$; $\eta^2_P = 0.08$), the 'salience' network ($F(2,98) = 7.68$; $P = 0.0036$; $\eta^2_P = 0.07$), the 'self-reference' integrative network ($F(2,146) = 9.33$; $P = 0.0001$; $\eta^2_P = 0.06$) and the 'emotional' network ($F(2,172) = 9.04$; $P = 0.0001$; $\eta^2_P = 0.05$) (see *Methods* for the description of each network). Thus, the cortico-cortical phase-coherence values between any given network and the five others were significantly decreased during delta PS as compared with rapid PS. The pattern of cortico-cortical phase coherence when comparing delta PS with wake was more complex, with a decrease of coherence in some areas/networks but not in others (Fig. 4). During wakefulness, cortico-cortical phase coherence was decreased relative to rapid PS for posterior insula, auditory, integrative and emotional

networks (Fig. 4*A*). There were also significant effects of frequency band for all networks, phase coherence on the delta band being always significantly higher than the others, and an effect of 'network' for all except the salience network. Details of these effects as well as interactions are described in Table 8.

Fig. 4*B* shows the correlation matrices of phase-coherence values in the delta band during wake, delta PS and rapid PS, for each brain area included in the functional networks. The number of couples of regions with significant coherence values (i.e. >0.2) was significantly lower during delta PS (11% of significant couples) as compared with both wake and rapid PS (27% and 30% of significant couples) ($P = 0.009$).

Delta/rapid *versus* tonic/phasic subdivisions of paradoxical sleep

Delta PS could incorporate both tonic and phasic periods, and the same was the case for rapid PS (Fig. 5). Within the 'tonic' PS periods, thalamo-cortical phase coherences were significantly lower in periods of delta PS as compared with rapid PS (0.19 (0.2) *vs.* 0.22 (0.23)) ($F(1,56) = 14.45$; $P = 0.0004$; $\eta^2_p = 0.21$). A significant

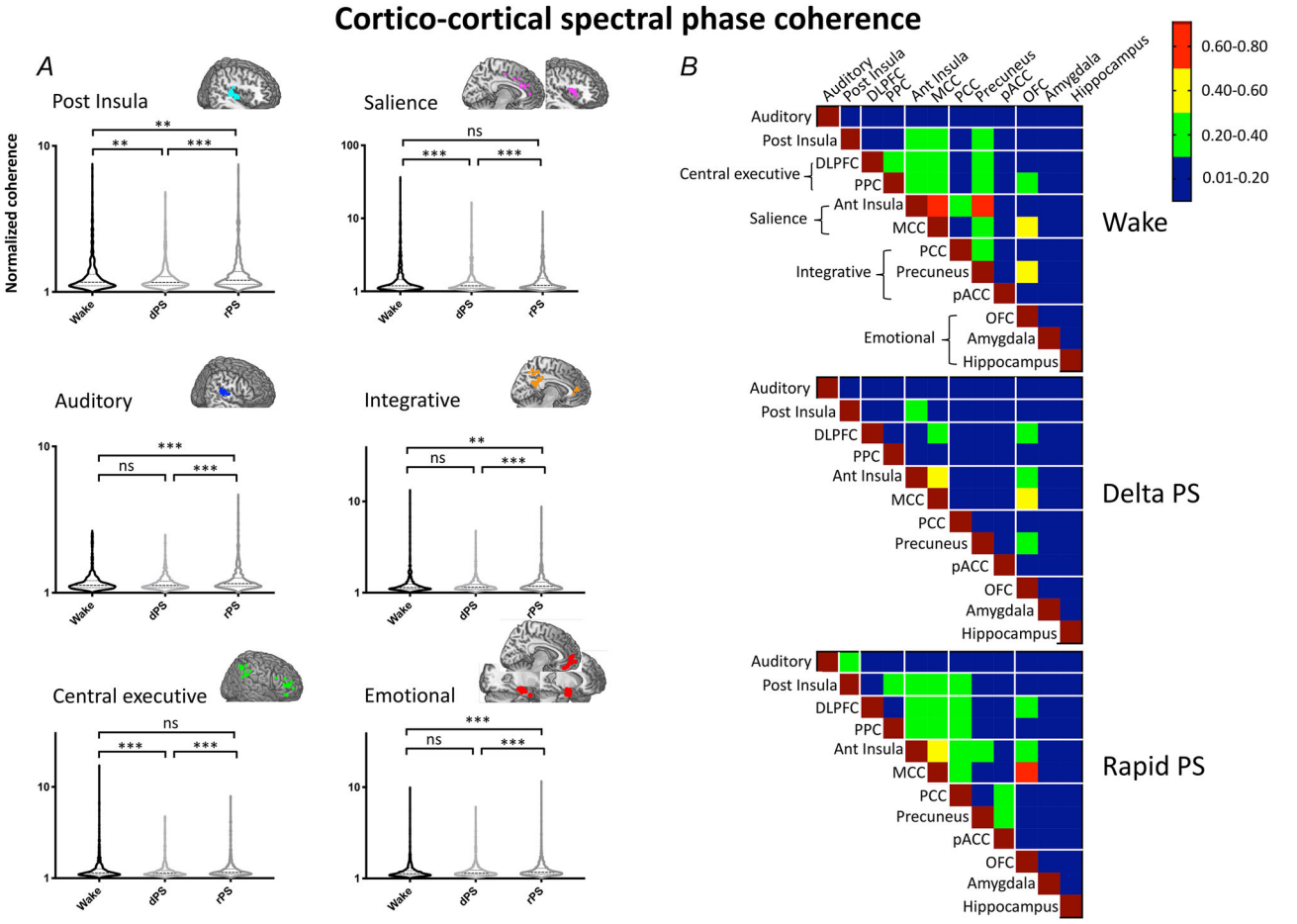

Figure 4. Cortico-cortical spectral phase coherences
A, violin plots of antilog normalized phase-coherence values during wake, delta paradoxical sleep (PS) and rapid PS with other sensory areas/networks for posterior insula (n = 605), auditory cortex (n = 540), central executive (n = 700), salience (n = 600), integrative (self-reference) (n = 755) and emotional (n = 885). Cortico-cortical phase coherence was significantly decreased during delta PS as compared with rapid PS for all sensory areas/networks and as compared with wake for posterior insula, central executive and salience networks; phase coherence was also significantly decreased during waking as compared with rapid PS for posterior insula, auditory, integrative and emotional networks. *B*, mean phase-coherence values in the delta band during wake, delta PS and rapid PS of each area with the others. Auditory cortex, posterior insula, dorsolateral prefrontal cortex, posterior parietal cortex, anterior insula, mid-cingulate, posterior cingulate, precuneus, perigenual anterior cingulate, orbitofrontal cortex, amygdala, ventral hippocampus. The horizontal and vertical white lines delineate the sensory areas/networks to which these areas belong. The phase-coherence levels are represented from below 0.2 (dark blue) to 0.6–0.8 (red). Note that the levels of phase coherence are mostly lower during delta PS as compared with both wake and rapid PS.

effect of frequency band was also present ($F(4,56) = 14.88$; $P < 0.0001$; $\eta^2_P = 0.21$), without significant effect of network ($F(5,56) = 0.96$; $P = 0.44$), nor significant interactions.

Discussion

Periods of rhythmic delta activity in the posterior thalamus during paradoxical sleep were associated with decreased thalamo-cortical and cortico-cortical functional connectivity, both relative to the waking state and to periods of 'rapid' (non-delta) PS. The classification based on delta/rapid alternance did not overlap with the classically defined 'tonic/phasic' PS periods, since each of such periods (with or without REMs) could contain delta and rapid PS phases. This suggests that the rapid and delta phases represent a new and distinct dichotomy of functional states in PS, which might be relevant to understand some particularities of mental activity during this sleep stage.

Delta and rapid thalamic activities define functionally distinct states within PS

Neuronal coherence is thought to reflect a fundamental mechanism of communication in mammalian brains, from rodents to humans (Mondino et al., 2020; Myers et al., 2022), and its estimation via the spectral analysis of EEG signals is a robust measure of functional connectivity between brain regions (Nunez et al., 2015; Paquola et al., 2020). Being based on the stability of phase relations between signals, spectral coherence may be considered largely independent of the amplitude of the signal and can reach high values despite a drop in amplitude of one of them. The striking suppression of spectral phase coherence observed during thalamic delta PS suggests that both thalamo-cortical and cortico-cortical relationships were disrupted during most of the time that the brain spends in PS, as delta thalamic periods represent ~70% of PS duration (Magnin et al 2004).

Failure of adequate functional connectivity during PS has been previously reported using both functional imaging and electrophysiology (Braun, 1997; Chow et al., 2013; Corsi-Cabrera, 2003; Corsi-Cabrera et al., 2008; Nir & Tononi, 2010), reviewed by Shine et al. (2023). These studies suggested that the thalamus may act as a connector hub in the network organization of the brain (Hwang et al., 2017), changing its functional connectivity with the cortex during wake/sleep and sleep/wake transitions (Hale et al., 2016; Larson-Prior et al., 2011; Picchioni et al., 2014; Setzer et al., 2022; Spoormaker et al., 2010). However, this is to our knowledge the first study showing that such a drop of functional connectivity occurs at specific PS sub-periods; namely, those characterized

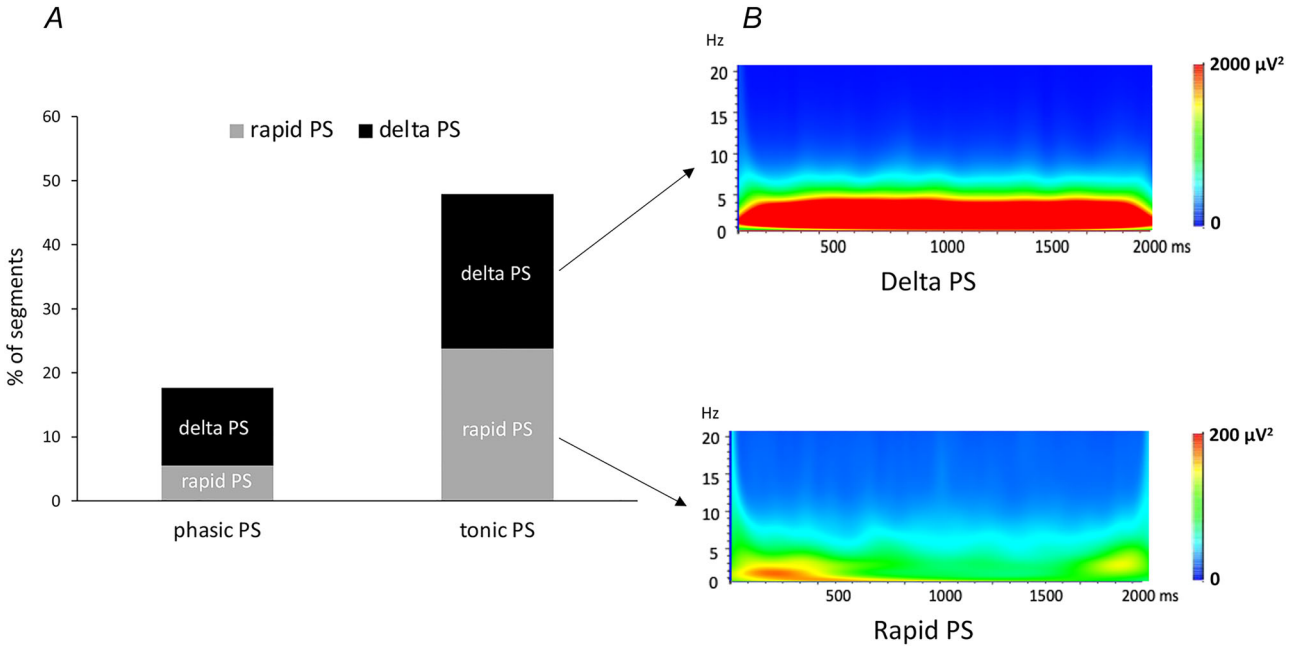

Figure 5. Percentages of rapid PS and delta PS segments within phasic and tonic periods of PS
A, percentages of rapid paradoxical sleep (PS) and delta PS segments within phasic and tonic periods of PS. Note that in both tonic and phasic PS there are rapid and delta periods indicating that the two classification modes (tonic/phasic and delta/rapid) do not overlap. *B*, grand means of time frequency signals of thalamus in delta PS (*top*) and rapid PS (*bottom*), all within tonic PS. Note the difference in colour scale during delta PS (2000 μV^2) and rapid PS (200 μV^2).

Table 8. Three-factor ANOVA for networks' spectral phase coherences between each of the different functional networks and the others. F, *P* and η^2_p values

Network	State of vigilance	Network	Band	State*N	Network*B	State*B	S*B*N
Posterior insula	(2,116) = 16.60; **<0.0001; 0.13**	(4,116) = 4.99; **0.0010; 0.15**	(4,116) = 63.4; **<0.0001; 0.35**	(8,232) = 1.95; 0.0534	(16,464) = 3.07; **<0.0001; 0.04**	(8,232) = 4.55; **<0.0001; 0.04**	(32,928) = 0.79; 0.79
Auditory cortex	(2,103) = 16.66; **<0.0001; 0.14**	(4,103) = 6.68; **<0.0001; 0.21**	(4,103) = 73.38; **<0.0001; 0.42**	(8,206) = 1.06; 0.40	(16,412) = 2.92; **0.0001; 0.05**	(8,206) = 4.51; **<0.0001; 0.04**	(32,824) = 0.81; 0.77
Central executive	(2,135) = 12.20; **<0.0001; 0.08**	(4,135) = 3.81; **0.0057; 0.10**	(4,135) = 82.73; **<0.0001; 0.38**	(8,270) = 1.19; 0.31	(16,540) = 2.96; **<0.0001; 0.04**	(8,270) = 3.13; **0.0017; 0.02**	(32,1080) = 0.45; 0.99
Salience	(2,98) = 7.68; **0.0006; 0.07**	(4,98) = 2.41; 0.054	(4,98) = 54.57; **<0.0001; 0.36**	(8,196) = 1.03; 0.41	(16,392) = 1.55; 0.079	(8,196) = 3.62; **0.0004; 0.04**	(32,784) = 0.68; 0.91
Integrative ('self-reference')	(2,146) = 9.33; **0.0001; 0.06**	(4,146) = 5.82; **0.0002; 0.14**	(4,146) = 91.12; **<0.0001; 0.38**	(8,292) = 1.03; 0.41	(16,584) = 3.89; **<0.0001; 0.06**	(8,292) = 6.56; **<0.0001; 0.03**	(32,1168) = 0.78; 0.81
Emotional	(2,172) = 9.04; **0.0001; 0.05**	(4,172) = 6.30; **<0.0001; 0.20**	(4,172) = 42.33; **<0.0001; 0.13**	(8,344) = 0.33; 0.95	(16,688) = 2.02; 0.01	(8,344) = 0.86; 0.55	(32,1376) = 0.40; 0.99

by sequences of thalamic rhythmic slow delta waves. Depression of functional connectivity in PS has been considered to contribute to the bizarreness of dreams (Hobson, 2004), which are characterized by a discordance between the detail and precision with which sensory items are perceived (voices, faces, physical features), and the incongruence of the context in which such representations are embedded. A tight link between retrieval of perceptual items and retrieval of the context where they occurred ('item–context binding') is essential for the correct recovery of episodic memories, and needs oscillatory coupling between brain processing areas (Ekstrom & Yonelinas, 2020; Hanslmayr et al., 2016). Disruption of such binding during delta PS, as reflected by the drop of functional connectivity between sensory, limbic and high-order association areas, is likely to alter the retrieval of episodic memories and lead to the item–context disconnection that characterizes the content of dreams. Since delta thalamic activity occupies about 70% of total PS duration, the probability that dreams occur during periods of altered cortico-cortical spectral coherence is much greater than chance. But in parallel, the fact that functional connectivity remains high in ∼30% of PS time ('rapid PS') also implies that during these rapid periods item–context binding mechanisms may remain appropriate. This might be linked to the frequent occurrence within dreams of periods with perfectly congruent scenes, which are disrupted by the sudden intrusion of abnormal contextual elements.

Periods of thalamic delta rhythmic waves were most prominent in the PuM, as previously reported (Magnin et al., 2004), although they have also been described in other posterior nuclei; for instance, the central lateral in the present study and the ventro-caudalis and centro-median nuclei in the study of Velasco et al. (1979). While it remains unknown to what extent such rhythmic delta waves can invade other parts of the thalamus, recent data suggest their absence in the anterior thalamic nuclei (Simor et al., 2021; Szabó et al., 2022). The PuM is a large, associative thalamic nucleus, which does not receive input from the periphery but shows instead reciprocal connections with virtually all cortical regions (reviews in Benarroch, 2015; Froesel et al., 2021; Shipp, 2003). By receiving input from cortical layers and projecting to other cortical regions, associative thalamic nuclei such as the PuM represent a privileged trans-thalamic route for rapid cortico-cortical information transfer (Cappe et al., 2009; Sampathkumar et al., 2021; Sherman, 2007; Vittek et al., 2023), giving rise to the 'replication principle', whereby for each direct cortico-cortical pathway there is an indirect cortico-thalamo-cortical route (Froesel et al., 2021; Halassa & Sherman, 2019; Shipp, 2003). Indeed, if two cortical areas communicate directly, they are also likely to have overlapping thalamic fields (Baleydier & Mauguière, 1987; Shipp, 2003), and the PuM connection

zones of nearby cortical areas overlap (Sherman, 2007), allowing transcortical communication via the thalamus. Thalamic nuclei can therefore coordinate cortical information processing by facilitating the formation of synchronized trans-areal assemblies (Nakajima & Halassa, 2017; Sherman, 2007; Shipp, 2003). Therefore, the drastic drop of cortico-cortical phase coherence during delta PS periods may not merely reflect a loss of direct cortico-cortical transfers, but also and especially the inability of modulatory thalamic nodes to ensure trans-thalamic cortico-cortical functional connectivity during these episodes.

Frequency-specificity of spectral phase coherence decrease

Functional connectivity changes were especially pronounced in the low- and mid-regions of the spectrum (delta, theta and alpha) relative to the rapid beta and gamma bands. This is consistent with a disruption in long-range inter-areal communication, which is mainly sustained by this range of frequencies (1–12 Hz), whereas the high-frequency bands (gamma) are predominantly involved in short-distance synchronization (Kopell et al., 2000; Myers et al., 2022; von Stein et al., 2000). In human intracranial studies, gamma band coherence predominates for signals arising very near to the recording electrodes, whereas phase coherence for slower signals (1–5 Hz) is higher for signals further away (Bourdillon et al., 2020; Myers et al., 2022). In both rodents and humans, theta and delta oscillations can act as 'carriers' of more rapid frequencies (Axmacher et al., 2010; Colgin et al., 2009; Maris et al., 2011), which not only allows high frequencies to be transmitted at distances they would not reach by themselves, but also enables different high-frequency (e.g. gamma) cycles to be nested within a single low-frequency cycle, hence permitting multiple neural codes to be represented and transmitted in a defined order (Staudigl & Hanslmayr, 2013). In the present study, maximal drop in phase coherence occurred in the delta frequency range (Fig. 3*C*), which is also the one showing the strongest 'carrier' effects in humans (Hanslmayr et al., 2016).

Decoupling of thalamic and cortical delta activity during PS

Other instances of cortical delta EEG waves have been described during human PS; in particular, the so-called 'sawtooth waves' (Bernardi et al., 2019; Frauscher et al., 2020). It is, however, unlikely that these activities could be a counterpart of the thalamic delta periods described here, since the duration of cortical 'sawtooth' bursts amounts to less than 5% of the total PS duration (Frauscher et al., 2020), whereas the delta thalamic periods represent more than half of total PS time. Also, the 'sawtooth' cortical waves have been associated with a concomitant increase in high-frequency gamma in sensory, associative and limbic areas (Bernardi et al., 2019; Frauscher et al., 2020; Peter-Derex et al., 2023) – something that did not occur in the present study (see Fig. 1). Therefore, while cortical delta 'sawtooth' bursts appear as possible 'microstates' within PS (Frauscher et al., 2020), thalamic delta PS periods represent long-lasting *macro-states* which may influence thalamo-cortical function during tens of seconds. The decrease of thalamo-cortical spectral phase coherence during delta PS also implies that the prominent thalamic slow waves in this period were not functionally transmitted to, nor received from, the cortex. In this respect, delta waves in PS greatly differ from delta waves in slow-wave sleep, which are generated by a highly coherent thalamo-cortical network and are therefore reflected in cortical activity (Crunelli et al., 2015). Delta waves in PS appear rather limited to thalamic level and hardly, if at all, transmitted to the cortex.

Particularities in the neurotransmitters involved in PS may underlie the lack of thalamo-cortical transmission of PS delta waves. Brain activation during PS is mainly ensured by an excitatory effect of acetylcholine on cerebral structures instead of the brainstem monoaminergic input which predominate during waking (Steriade, 2004). However, acetylcholine has a specific paradoxical inhibitory effect on cells of the thalamic reticular nucleus, which leads to their hyperpolarization (Marks & Roffwarg, 1991; McCormick & Prince, 1986). These cells being endowed with rhythmic properties in the slow-frequency range when hyperpolarized (Fuentealba & Steriade, 2005), they generate delta rhythmic field potentials (Ben-Ari et al., 1976; Dingledine & Kelly, 1977). At the same time, thalamic relay cells driving activity toward the cortex are activated by acetylcholine, which prevents them from entering in a similar rhythmic firing mode, hence providing a putative explanation for why the post-synaptic slow field potentials recorded at the thalamic level do not find an obvious counterpart at cortical level.

Delta and rapid PS differ from tonic and phasic periods

In their seminal description, Velasco et al (1979) reported that PS-related thalamic delta periods were not associated with the ocular movements of phasic PS, which is not surprising given the dissimilar duration of the short phasic periods and long-lasting delta thalamic activity. Here we also show the independence of delta thalamic phases relative to tonic PS, which constitute most of the PS time. As shown in Fig. 5, tonic PS periods could coexist with either delta or rapid thalamic activity, and only during delta thalamic periods was thalamo-cortical

phase coherence decreased. The presence or absence of a rhythmic thalamic delta activity appears therefore to determine a distinct dichotomy within PS, not overlapping with other dichotomic states (tonic/phasic; sawtooth waves, etc).

Limitations and perspectives of the study

Our results were obtained in epileptic patients, whose brain activity cannot be fully extrapolated to the general population. However, the original description of delta PS activity concerned non-epileptic subjects treated for tremor or rigidity (Velasco et al., 1979), thus allowing a certain generalization. Data from regions involved in epileptic discharges were scrupulously excluded from our analyses, and we also inspected MRI scans to rule out structural abnormalities, particularly in temporal and hippocampal regions which are known to be the most common epileptic areas. Most of the patients were on anti-epileptic drugs, which may alter brain metabolism and induce impairments in brain network connectivity (van Veenendaal et al., 2017). Notwithstanding this difficulty, the results reported here are based on intra-individual comparisons across vigilance states. Hence, we believe that the changes in phase coherence are robust and reliable. Without a stimulus or signal providing a 'time zero' point, the analysis with spectral phase coherence does not allow us to determine the directionality of the connectivity between different signals, and this can be considered a limitation of the study. Our aim, however, was not to assess the directionality of the relationship, but rather whether such relationship varied according to the type of activity in the thalamic nuclei investigated. Also, since coherence in different areas was pooled within a given network, differences in coherence between networks could be due to just one of its pertaining regions, the grand mean being driven by this region alone, whereas we interpret it as a network effect.

The need to ensure stable recording periods during night sleep prevented us from iteratively awakening the participants to verify their dream reports. The relationship between thalamo-cortical connectivity and dream content therefore remains speculative and is clearly one limitation of this study. Since intrathalamic iEEG recordings in humans are extremely rare, this limitation may prove very difficult to overcome unless advances in the processing of scalp EEG signals in the future allow a non-invasive determination of whether the thalamus is in delta or rapid PS mode of activity.

Conclusion

We report a decrease in both thalamo-cortical and cortico-cortical functional connectivity during a specific phase of paradoxical sleep characterized by sequences of delta thalamic activity, dissociated from rapid activity within the cortex. Intracranial iEEG data with electrodes implanted both in thalamus and cortex may contribute to fill some conceptual gap in previous studies focused exclusively on cortico-cortical connectivity during this sleep stage. This approach constitutes a robust physiological basis for the understanding of mechanisms underlying oneiric activity.

References

Achermann, P., & Borbély, A. A. (1998). Coherence analysis of the human sleep electroencephalogram. *Neuroscience*, **85**(4), 1195–1208.

Arnulf, I. (2012). REM sleep behavior disorder: Motor manifestations and pathophysiology. *Movement Disorders*, **27**(6), 677–689.

Aserinsky, E., & Kleitman, N. (1953). Regularly occurring periods of eye motility, and concomitant phenomena, during sleep. *Science*, **118**(3062), 273–274.

Axmacher, N., Henseler, M. M., Jensen, O., Weinreich, I., Elger, C. E., & Fell, J. (2010). Cross-frequency coupling supports multi-item working memory in the human hippocampus. *Proceedings of the National Academy of Sciences of the United States of America*, **107**(7), 3228–3233.

Baleydier, C., & Mauguiere, F. (1985). Anatomical evidence for medial pulvinar connections with the posterior cingulate cortex, the retrosplenial area, and the posterior parahippocampal gyrus in monkeys. *Journal of Comparative Neurology*, **232**(2), 219–228.

Baleydier, C., & Mauguière, F. (1987). Network organization of the connectivity between parietal area 7, posterior cingulate cortex and medial pulvinar nucleus: A double fluorescent tracer study in monkey. *Experimental Brain Research*, **66**(2), 385–393.

Bastuji, H., Frot, M., Mazza, S., Perchet, C., Magnin, M., & Garcia-Larrea, L. (2016). Thalamic responses to nociceptive-specific input in humans: Functional dichotomies and thalamo-cortical connectivity. *Cerebral Cortex*, **26**(6), 2663–2676.

Ben-Ari, Y., Dingledine, R., Kanazawa, I., & Kelly, J. S. (1976). Inhibitory effects of acetylcholine on neurones in the feline nucleus reticularis thalami. *The Journal of Physiology*, **261**(3), 647–671.

Benarroch, E. E. (2015). Pulvinar: Associative role in cortical function and clinical correlations. *Neurology*, **84**(7), 738–747.

Bernardi, G., Betta, M., Ricciardi, E., Pietrini, P., Tononi, G., & Siclari, F. (2019). Regional delta waves in human rapid eye movement sleep. *Journal of Neuroscience*, **39**(14), 2686–2697.

Bourdillon, P., Hermann, B., Guénot, M., Bastuji, H., Isnard, J., King, J.-R., Sitt, J., & Naccache, L. (2020). Brain-scale cortico-cortical functional connectivity in the delta-theta band is a robust signature of conscious states: An intracranial and scalp EEG study. *Scientific Reports*, **10**(1), 14037.

Braun, A. (1997). Regional cerebral blood flow throughout the sleep-wake cycle. An H2(15)O PET study. *Brain*, **120**(Pt 7), 1173–1197.

Brown, R. E., Basheer, R., McKenna, J. T., Strecker, R. E., & McCarley, R. W. (2012). Control of sleep and wakefulness. *Physiological Reviews*, **92**, 1087–1187.

Cappe, C., Morel, A., Barone, P., & Rouiller, E. M. (2009). The thalamocortical projection systems in primate: An anatomical support for multisensory and sensorimotor interplay. *Cerebral Cortex*, **19**(9), 2025–2037.

Casaglia, E., & Luppi, P.-H. (2022). Is paradoxical sleep setting up innate and acquired complex sensorimotor and adaptive behaviours?: A proposed function based on literature review. *Journal of Sleep Research*, **31**(4), e13633.

Chow, H. M., Horovitz, S. G., Carr, W. S., Picchioni, D., Coddington, N., Fukunaga, M., Xu, Y., Balkin, T. J., Duyn, J. H., & Braun, A. R. (2013). Rhythmic alternating patterns of brain activity distinguish rapid eye movement sleep from other states of consciousness. *Proceedings National Academy of Science USA*, **110**(25), 10300–10305.

Colgin, L. L., Denninger, T., Fyhn, M., Hafting, T., Bonnevie, T., Jensen, O., Moser, M.-B., & Moser, E. I. (2009). Frequency of gamma oscillations routes flow of information in the hippocampus. *Nature*, **462**(7271), 353–357.

Corsi-Cabrera, M. (2003). Rapid eye movement sleep dreaming is characterized by uncoupled EEG activity between frontal and perceptual cortical regions. *Brain and Cognition*, **51**(3), 337–345.

Corsi-Cabrera, M., Guevara, M. A., & del Río-Portilla, Y. (2008). Brain activity and temporal coupling related to eye movements during REM sleep: EEG and MEG results. *Brain Research*, **1235**, 82–91.

Crunelli, V., David, F., Lőrincz, M. L., & Hughes, S. W. (2015). The thalamocortical network as a single slow wave-generating unit. *Current Opinion in Neurobiology*, **31**, 72–80.

Dalla Barba, G., Brazzarola, M., Barbera, C., Marangoni, S., Causin, F., Bartolomeo, P., & Thiebaut de Schotten, M. (2018). Different patterns of confabulation in left visuo-spatial neglect. *Experimental Brain Research*, **236**(7), 2037–2046.

Dingledine, R., & Kelly, J. S. (1977). Brain stem stimulation and the acetylcholine-evoked inhibition of neurones in the feline nucleus reticularis thalami. *The Journal of Physiology*, **271**(1), 135–154.

Doucet, G. E., Lee, W. H., & Frangou, S. (2019). Evaluation of the spatial variability in the major resting-state networks across human brain functional atlases. *Human Brain Mapping*, **40**(15), 4577–4587.

Dresler, M., Koch, S. P., Wehrle, R., Spoormaker, V. I., Holsboer, F., Steiger, A., Sämann, P. G., Obrig, H., & Czisch, M. (2011). Dreamed movement elicits activation in the sensorimotor cortex. *Current Biology*, **21**(21), 1833–1837.

Ekstrom, A. D., & Yonelinas, A. P. (2020). Precision, binding, and the hippocampus: Precisely what are we talking about? *Neuropsychologia*, **138**, 107341.

Faillenot, I., Heckemann, R. A., Frot, M., & Hammers, A. (2017). Macroanatomy and 3D probabilistic atlas of the human insula. *Neuroimage*, **150**, 88–98.

Fanselow, M. S., & Dong, H.-W. (2010). Are The Dorsal and Ventral Hippocampus functionally distinct structures? *Neuron*, **65**(1), 7.

Frauscher, B., von Ellenrieder, N., Dolezalova, I., Bouhadoun, S., Gotman, J., & Peter-Derex, L. (2020). Rapid eye movement sleep sawtooth waves are associated with widespread cortical activations. *Journal of Neuroscience*, **40**(46), 8900–8912.

Friedman, D. P., Murray, E. A., O'Neill, J. B., & Mishkin, M. (1986). Cortical connections of the somatosensory fields of the lateral sulcus of macaques: Evidence for a corticolimbic pathway for touch. *Journal of Comparative Neurology*, **252**(3), 323–347.

Froesel, M., Cappe, C., & Ben Hamed, S. (2021). A multisensory perspective onto primate pulvinar functions. *Neuroscience, & Biobehavioral Reviews*, **125**, 231–243.

Frot, M., Mauguière, F., & Garcia-Larrea, L. (2022). Insular dichotomy in the implicit detection of emotions in human faces. *Cerebral Cortex*, **32**(19), 4215–4228.

Fuentealba, P., & Steriade, M. (2005). The reticular nucleus revisited: Intrinsic and network properties of a thalamic pacemaker. *Progress in Neurobiology*, **75**(2), 125–141.

Halassa, M. M., & Sherman, S. M. (2019). Thalamocortical circuit motifs: A general framework. *Neuron*, **103**(5), 762–770.

Hale, J. R., White, T. P., Mayhew, S. D., Wilson, R. S., Rollings, D. T., Khalsa, S., Arvanitis, T. N., & Bagshaw, A. P. (2016). Altered thalamocortical and intra-thalamic functional connectivity during light sleep compared with wake. *Neuroimage*, **125**, 657–667.

Hanslmayr, S., Staresina, B. P., & Bowman, H. (2016). Oscillations and episodic memory: Addressing the synchronization/desynchronization conundrum. *Trends in Neuroscience (Tins)*, **39**(1), 16–25.

Heine, L., Soddu, A., Gómez, F., Vanhaudenhuyse, A., Tshibanda, L., Thonnard, M., Charland-Verville, V., Kirsch, M., Laureys, S., & Demertzi, A. (2012). Resting state networks and consciousness. *Frontiers in Psychology*, **3**, 295.

Hirai, T., & Jones, E. G. (1989). A new parcellation of the human thalamus on the basis of histochemical staining. *Brain Research Brain Research Reviews*, **14**(1), 1–34.

Hobson, A. (2004). A model for madness? *Nature*, **430**, 21–21.

Hobson, J. (1997). Dreaming as delirium: A mental status analysis of our nightly madness. *Seminars in Neurology*, **17**(2), 121–128.

Hobson, J. A. (2009). REM sleep and dreaming: Towards a theory of protoconsciousness. *Nature Reviews Neuroscience*, **10**(11), 803–813.

Hwang, K., Bertolero, M. A., Liu, W. B., & D'Esposito, M. (2017). The human thalamus is an integrative hub for functional brain networks. *Journal of Neuroscience*, **37**(23), 5594–5607.

John, Y. J., Bullock, D., Zikopoulos, B., & Barbas, H. (2013). Anatomy and computational modeling of networks underlying cognitive-emotional interaction. *Frontiers in Human Neuroscience*, **7**, 101.

Jouvet, M., Michel, F., & Courjon, J. (1959). [On a stage of rapid cerebral electrical activity in the course of physiological sleep]. *Comptes Rendus Des Seances De La Societe De Biologie Et De Ses Filiales*, **153**, 1024–1028.

Kopell, N., Ermentrout, G. B., Whittington, M. A., & Traub, R. D. (2000). Gamma rhythms and beta rhythms have different synchronization properties. *Proceedings National Academy of Science USA*, **97**(4), 1867–1872.

Krauth, A., Blanc, R., Poveda, A., Jeanmonod, D., Morel, A., & Székely, G. (2010). A mean three-dimensional atlas of the human thalamus: Generation from multiple histological data. *Neuroimage*, **49**(3), 2053–2062.

Larson-Prior, L. J., Power, J. D., Vincent, J. L., Nolan, T. S., Coalson, R. S., Zempel, J., Snyder, A. Z., Schlaggar, B. L., Raichle, M. E., & Petersen, S. E. (2011). Modulation of the brain's functional network architecture in the transition from wake to sleep. *Progress in Brain Research*, **193**, 277–294.

Luppi, P.-H., Clement, O., Sapin, E., Peyron, C., Gervasoni, D., Léger, L., & Fort, P. (2012). Brainstem mechanisms of paradoxical (REM) sleep generation. *Pflügers Archiv: European Journal of Physiology*, **463**(1), 43–52.

Magnin, M., Bastuji, H., Garcia-Larrea, L., & Mauguiere, F. (2004). Human thalamic medial pulvinar nucleus is not activated during paradoxical sleep. *Cerebral Cortex*, **14**(8), 858–862.

Magnin, M., Rey, M., Bastuji, H., Guillemant, P., Mauguière, F., & Garcia-Larrea, L. (2010). Thalamic deactivation at sleep onset precedes that of the cerebral cortex in humans. *Proceedings of the National Academy of Sciences of the United States of America*, **107**(8), 3829–3833.

Mahowald, M. W., & Schenck, C. H. (2004). Rem sleep without atonia–from cats to humans. *Archives Italiennes De Biologie*, **142**(4), 469–478.

Maris, E., van Vugt, M., & Kahana, M. (2011). Spatially distributed patterns of oscillatory coupling between high-frequency amplitudes and low-frequency phases in human iEEG. *Neuroimage*, **54**(2), 836–850.

Marks, G. A., & Roffwarg, H. P. (1991). Cholinergic modulation of responses to glutamate in the thalamic reticular nucleus of the anesthetized rat. *Brain Research*, **557**(1–2), 48–56.

McCormick, D. A., & Prince, D. A. (1986). Acetylcholine induces burst firing in thalamic reticular neurones by activating a potassium conductance. *Nature*, **319**(6052), 402–405.

Menon, V. (2011). Large-scale brain networks and psychopathology: A unifying triple network model. *Trends in Cognitive Sciences*, **15**(10), 483–506.

Mondino, A., Cavelli, M., González, J., Osorio, L., Castro-Zaballa, S., Costa, A., Vanini, G., & Torterolo, P. (2020). Power and coherence in the EEG of the Rat: Impact of behavioral states, cortical area, lateralization and light/dark phases. *Clocks Sleep*, **2**(4), 536–556.

Morel, A., Magnin, M., & Jeanmonod, D. (1997). Multiarchitectonic and stereotactic atlas of the human thalamus. *Journal of Comparative Neurology*, **387**(4), 588–630.

Myers, J. C., Smith, E. H., Leszczynski, M., O'Sullivan, J., Yates, M. J., McKhann, G., Mesgarani, N., Schroeder, C., Schevon, C., & Sheth, S. A. (2022). The spatial reach of neuronal coherence and spike-field coupling across the human neocortex. *Journal of Neuroscience*, **42**(32), 6285–6294.

Nakajima, M., & Halassa, M. M. (2017). Thalamic control of functional cortical connectivity. *Current Opinion in Neurobiology*, **44**, 127–131.

Nir, Y., & Tononi, G. (2010). Dreaming and the brain: From phenomenology to neurophysiology. *Trends in Cognitive Sciences*, **14**(2), 88–100.

Nunez, P. L., Srinivasan, R., & Fields, R. D. (2015). EEG functional connectivity, axon delays and white matter disease. *Clinical Neurophysiology*, **126**(1), 110–120.

Oudiette, D., Dodet, P., Ledard, N., Artru, E., Rachidi, I., Similowski, T., & Arnulf, I. (2018). REM sleep respiratory behaviours match mental content in narcoleptic lucid dreamers. *Scientific Reports*, **8**(1), 2636.

Paquola, C., Benkarim, O., DeKraker, J., Larivière, S., Frässle, S., Royer, J., Tavakol, S., Valk, S., Bernasconi, A., Bernasconi, N., Khan, A., Evans, A. C., Razi, A., Smallwood, J., & Bernhardt, B. C. (2020). Convergence of cortical types and functional motifs in the human mesiotemporal lobe. *Elife*, **9**, e60673.

Peever, J., & Fuller, P. M. (2017). The biology of REM sleep. *Current Biology*, **27**(22), R1237–R1248.

Peter-Derex, L., Avigdor, T., Rheims, S., Guénot, M., von Ellenrieder, N., Gotman, J., & Frauscher, B. (2023). Enhanced thalamocortical functional connectivity during REM sleep sawtooth waves. *Sleep*, **46**(6), zsad097.

Picchioni, D., Pixa, M. L., Fukunaga, M., Carr, W. S., Horovitz, S. G., Braun, A. R., & Duyn, J. H. (2014). Decreased connectivity between the thalamus and the neocortex during human nonrapid eye movement sleep. *Sleep*, **37**(2), 387–397.

Rorden, C., & Brett, M. (2000). Stereotaxic display of brain lesions. *Behavioural Neurology*, **12**(4), 191–200.

Rosenberg, D. S., Mauguiere, F., Demarquay, G., Ryvlin, P., Isnard, J., Fischer, C., Guenot, M., & Magnin, M. (2006). Involvement of medial pulvinar thalamic nucleus in human temporal lobe seizures. *Epilepsia*, **47**(1), 98–107.

Sampathkumar, V., Miller-Hansen, A., Sherman, S. M., & Kasthuri, N. (2021). Integration of signals from different cortical areas in higher order thalamic neurons. *Proceedings of the National Academy of Sciences of the United States of America*, **118**(30), e2104137118.

Saper, C. B., Fuller, P. M., Pedersen, N. P., Lu, J., & Scammell, T. E. (2010). Sleep state switching. *Neuron*, **68**(6), 1023–1042.

Schnider, A., Gutbrod, K., Hess, C. W., & Schroth, G. (1996). Memory without context: Amnesia with confabulations after infarction of the right capsular genu. *Journal of Neurology, Neurosurgery, and Psychiatry*, **61**(2), 186–193.

Schwartz, S., & Maquet, P. (2002). Sleep imaging and the neuro-psychological assessment of dreams. *Trends in Cognitive Sciences*, **6**(1), 23–30.

Seeley, W. W. (2010). Anterior insula degeneration in frontotemporal dementia. *Brain Structure and Function*, **214**(5–6), 465–475.

Setzer, B., Fultz, N. E., Gomez, D. E. P., Williams, S. D., Bonmassar, G., Polimeni, J. R., & Lewis, L. D. (2022). A temporal sequence of thalamic activity unfolds at transitions in behavioral arousal state. *Nature Communications*, **13**(1), 5442.

Sherman, S. M. (2007). The thalamus is more than just a relay. *Current Opinion in Neurobiology*, **17**(4), 417–422.
Shine, J. M., Lewis, L. D., Garrett, D. D., & Hwang, K. (2023). The impact of the human thalamus on brain-wide information processing. *Nature Reviews Neuroscience*, **24**(7), 416–430.
Shipp, S. (2003). The functional logic of cortico–pulvinar connections. *Philosophical Transactions of the Royal Society of London Series B, Biological Sciences*, **358**(1438), 1605–1624.
Simor, P., Peigneux, P., & Bódizs, R. (2023). Sleep and dreaming in the light of reactive and predictive homeostasis. *Neuroscience & Biobehavioral Reviews*, **147**, 105104.
Simor, P., Szalárdy, O., Gombos, F., Ujma, P. P., Jordán, Z., Halász, L., Erőss, L., Fabó, D., & Bódizs, R. (2021). REM sleep microstates in the human anterior thalamus. *Journal of Neuroscience*, **41**(26), 5677–5686.
Simor, P., van der Wijk, G., Nobili, L., & Peigneux, P. (2020). The microstructure of REM sleep: Why phasic and tonic? *Sleep Medicine Reviews*, **52**, 101305.
Spoormaker, V. I., Schroter, M. S., Gleiser, P. M., Andrade, K. C., Dresler, M., Wehrle, R., Samann, P. G., & Czisch, M. (2010). Development of a large-scale functional brain network during human non-rapid eye movement sleep. *Journal of Neuroscience*, **30**(34), 11379–11387.
Staudigl, T., & Hanslmayr, S. (2013). Theta oscillations at encoding mediate the context-dependent nature of human episodic memory. *Current Biology*, **23**(12), 1101–1106.
von Stein, A., Chiang, C., & König, P. (2000). Top-down processing mediated by interareal synchronization. *Proceedings National Academy of Science USA*, **97**(26), 14748–14753.
Steriade, M. (2004). Acetylcholine systems and rhythmic activities during the waking–sleep cycle. In Progress in Brain Research, *Acetylcholine in the Cerebral Cortex* (pp. 179–196). Elsevier. https://www.sciencedirect.com/science/article/pii/S0079612303450139
Szabó, J. P., Fabó, D., Pető, N., Sákovics, A., & Bódizs, R. (2022). Role of anterior thalamic circuitry during sleep. *Epilepsy Research*, **186**, 106999.
Uddin, L. Q., Yeo, B. T. T., & Spreng, R. N. (2019). Towards a universal taxonomy of macro-scale functional human brain networks. *Brain Topography*, **32**(6), 926–942.
van Veenendaal, T. M., IJff, D. M., Aldenkamp, A. P., Lazeron, R. H. C., Hofman, P. A. M., de Louw, A. J. A., Backes, W. H., & Jansen, J. F. A. (2017). Chronic antiepileptic drug use and functional network efficiency: A functional magnetic resonance imaging study. *World Journal of Radiology*, **9**(6), 287–294.
Velasco, M., Velasco, F., & Cepeda, C. (1979). A peculiar rhythmic EEG activity from ventrobasal thalamus during paradoxical sleep in man. *Electroencephalography and Clinical Neurophysiology*, **47**(2), 119–125.
Vittek, A.-L., Juan, C., Nowak, L. G., Girard, P., & Cappe, C. (2023). Multisensory integration in neurons of the medial pulvinar of macaque monkey. *Cerebral Cortex*, **33**(8), 4202–4215.
Wang, Z., Fei, X., Liu, X., Wang, Y., Hu, Y., Peng, W., Wang, Y., Zhang, S., & Xu, M. (2022). REM sleep is associated with distinct global cortical dynamics and controlled by occipital cortex. *Nature Communications*, **13**(1), 6896.
Whitfield-Gabrieli, S., Moran, J. M., Nieto-Castañón, A., Triantafyllou, C., Saxe, R., & Gabrieli, J. D. E. (2011). Associations and dissociations between default and self-reference networks in the human brain. *Neuroimage*, **55**(1), 225–232.

Additional information

Data availability statement

Data are available upon request to the authors.

Competing interests

The authors declare no competing financial interests.

Author contributions

H.B., M.M. and L.G-L. designed the research; H.B. and M.D. performed the research; H.B., M.D. and L.G-L. analysed the data; H.B., M.M. and L.G.-L. wrote the paper.

Funding

Supported by the LABEX CORTEX (ANR-11-LABX-0042; ANR-11-IDEX-0007), a Region Rhone-Alpes/France ARC2 2012−2015 scholarship and a INSERM Interface Grant to H.B.

Keywords

connectivity, human, intracerebral EEG, paradoxical (REM) sleep, thalamus

Supporting information

Additional supporting information can be found online in the Supporting Information section at the end of the HTML view of the article. Supporting information files available:

Peer Review History